Chinese Journal of Aeronautics, 2013,26(1): 27–36

Chinese Society of Aeronautics and Astronautics
& Beihang University

Chinese Journal of Aeronautics

cja@buaa.edu.cn
www.sciencedirect.com

Research on vacuum plume and its effects

He Bijiao, Zhang Jianhua, Cai Guobiao *

School of Astronautics, Beihang University, Beijing 100191, China

Received 14 October 2011; revised 14 December 2011; accepted 23 April 2012
Available online 16 January 2013

KEYWORDS

Attitude control;
Effects;
Experiments;
Monte Carlo methods;
Vacuum plume

Abstract In vacuum environment, the exhaust flow of attitude control thrusters would expand freely and produce the plume, which possibly causes undesirable contamination, aerodynamic force and heating effects to the spacecraft. Plume work station (PWS) is developed by Beihang University (BUAA) for numerically simulating the vacuum plume and its effects. An approach which combines the direct simulation Monte Carlo (DSMC) method and difference solution of Navier–Stokes (N–S) equations is applied. The internal flows in nozzles are simulated by solving the NS equations. The flow parameters at nozzle exit are used as the inlet boundary condition for the DSMC calculation. Experimental studies are carried out in a supersonic low density wind tunnel which could simulate the 60–80 km altitude environment to investigate the plume and its effects. To demonstrate the capability of PWS, numerical simulations are performed for the vacuum plume of several typical attitude control thrusters. The research results are of great help for the engineering design.

1. Introduction

In vacuum environment, the exhaust flow of the attitude control thrusters of satellites, spaceships, space stations and deep-space probes would expand freely and produce the plume. The vacuum plume would possibly cause undesirable contamination, aerodynamic force and thermal effects on the spacecraft, which would debase the capability of functional components and even make the flight missions fail. Therefore, for spacecraft designers the effects of the plume must be taken into account.

Vacuum plume would expand and form backflow behind the thruster. In many cases, vacuum plume backflow would probably impinge on the spacecraft surfaces. Plume effects consist of plume contamination, aerodynamic force and heating effects. For those spacecraft which use the electrical engines, plume effects even include electromagnetic effects.

Plume contamination would reduce the sensitivity of sensitive components, such as temperature-controlled surfaces, optical equipment and solar battery panels. Meanwhile, plume aerodynamic force effects would directly affect the attitude control of the spacecraft and cause more efforts to keep the spacecraft in normal attitude and position. Plume aerodynamic heating effects make spacecraft work in a high temperature environment, which may cause erratic action and poor performance. Finally, plume would contaminate the viewport of spacecraft and affect the target acquisition tasks, and even lead the tracking instruments to a morass of wrong judgments.

There are several accidents caused by plume effects. During the mission of the U.S. "Gemini" manned spacecraft, because no protective covers were used, the observation windows of this spacecraft suffered serious plume sediment contamination. Another accident happened during the service of the Japanese "BSE-1" satellite which was launched by the United States.

* Corresponding author. Tel.: +86 10 82336533.
E-mail address: cgb@buaa.edu.cn (G. Cai).

Peer review under responsibility of Editorial Committe of CJA.

ELSEVIER Production and hosting by Elsevier

1000-9361 © 2013 CSAA & BUAA. Production and hosting by Elsevier Ltd. Open access under CC BY-NC-ND license.
http://dx.doi.org/10.1016/j.cja.2012.12.016

The plume of this satellite's attitude control thrusters contaminated the solar cell surface and reduced the power of solar cells. Besides, in the U.S. "Voyager" Spacecraft, several 0.9 N rocket motors were used for orbit adjustments. The flight data showed that the plume impact resulted in a 22% drop in the motor's average thrust and a 60% drop in torque of the satellite. Although some preventive measures were originally introduced to reduce the plume's direct contaminations and impingements, the design still could not protect the satellite from the plume impacts. Moreover, the plume contamination also caused a poor performance of the tracking instrument in Mariner 10. Though Mariner 10 recovered its normal function through a series of spacecraft adjustments, the control system consumed incidental fuel and shortened the lifespan.

Vacuum plume covers all the continuum, transition, and free molecular flow regions. Continuum flow is located in the core area of plume. Transition flow and free molecular flow are in the far areas of plume. Therefore, vacuum plume could not be described by one mathematical model alone. For Continuum flow, the governing equations are the N–S equations. For the free molecular flow, the governing equation is the Boltzmann equation without the collision factor. However, for the transition flow, the governing equation is the full Boltzmann equation. The Boltzmann equation is a nonlinear integro-differential equation, which has analytical solution only for few special cases of collisionless or spatial homogeneous problems.

Until now three kinds of methods are introduced to research the vacuum plume and its effects. The first one refers to the semi-experimental and analytical methods, which include the Simons method[1] and MOC method.[2] These methods have relatively high efficiency but low accuracy and are only suitable for simple cases. The second kind is the numerical simulation method. In the early 1960s, Bird proposed the DSMC method,[3] which directly simulates the physical phenomena described by the Boltzmann equation. Since the appearance of the DSMC method, it has been successfully applied to a wild range of high-altitude rarefied gas dynamics problems.[4] The third one belongs to experimental study, which contains simulation experiments on the ground and flight experiments. Ground simulation experiments[5,6] are often used to validate the numerical simulation programs and also used to measure small thruster plume parameters.[7] Flight experiments can obtain the actual conditions of the plume. A flight experiment named SPIFEX was conducted to research plume effects by the U.S. space shuttle.[8] However, the cost of flight experiment is too expensive.

The research of plume started in the 1960s. A lot of experimental researches were performed in recent years.[9,10] With the advanced computation development, numerical simulation becomes a main tool for the plume study.[11–13] The plume question could be understood more distinctly by combining experimental study and numerical simulation.

This paper introduces all the investigations of vacuum plume and its effects, which are conducted in Beihang University (BUAA). The investigations include the numerical simulations and experimental studies. The remainder of the paper is organized as follows: firstly the numerical simulation methods and Plume WorkStation (PWS) software are introduced. Then experiments are carried out to validate PWS and study the plume aerodynamic force and heating effects.

2. Computation scheme

2.1. Nozzle solution

The governing equations of the nozzle simulation are the compressible and turbulent N–S equations, ignoring the factors of force and radiation. The equations in the computational system can be written as

$$\frac{\partial Q}{\partial t}+\frac{\partial F}{\partial x}+\frac{\partial G}{\partial y}=\frac{\partial F_{\mathrm{v}}}{\partial x}+\frac{\partial G_{\mathrm{v}}}{\partial y}+S \tag{1}$$

where G is the conservative quantity, F and G are the inviscous fluxes, F_{v} and G_{v} are the viscous fluxes and S is the source term.

Baldwin and Lomax algebraic model[14] is the famous turbulence model and is adopted for the nozzle turbulent flow calculation. The computation mesh is generated by using algebraic method. Grid mesh at the boundary layer and the nozzle throat is refined in order to reveal drastic changes of the flow. The explicit MacCormack prediction-correction structure is used. Forward differential scheme is adopted in the prediction step and backward differential is adopted in the correction step. Mesh spacing in the computation is equal to 1. Half of the computation domain is calculated because of field symmetry. The four boundary conditions are the nozzle inlet, nozzle exit, the nozzle axis, and the solid wall.

2.2. Plume solution

The pressure and density at the nozzle exit section of the attitude control thrusters are relatively low. So the DSMC method can be applied to simulating vacuum plume entirely outside the nozzle.

2.2.1. Governing equation

The direct simulation Monte Carlo (DSMC) method is a direct simulation method for rarefied gas dynamics.[15] In DSMC calculation, the flow domain is first divided into a number of cells. Then the computational particles are placed into the cells. All particles carry information of position, velocity, internal energy and weight factor. During each time step, the treatment of all particles is performed by two loops. The outer loop extends over all grid cells in which all particles move and interact with the boundary surfaces; the inner loop extends over the particles within a cell in which particles collide with each other.

When the molecule collisions are simulated, two possible collision particles are randomly selected firstly and then are sampled according to the collision probability, which is in direct proportion to the relative velocity of particle pair.

There are many published schemes for collision sampling, such as time counter method,[3] Null-collision method,[16] collision frequency method,[17] main frequency method,[18] no time counter method[19] and randomly sampled frequency (RSF) method.[20] The RSF method used in this paper selects a small amount of particles to simulate the collisions and overcomes the disadvantage of excessive memory consumption. It is proved that the RSF method has the same efficiency as TC method.

The calculation boundaries contain object surface, inflow boundary, outflow boundary and symmetry boundary for axisymmetric simulation. In the simulation, the following boundary problems should be considered:

Symmetry boundary condition: no simulation particle is allowed to move across the axis.

Outflow boundary condition: when it crosses the outflow boundary, a particle should be discarded.

New particle generation: at the inflow boundary the simulation particles are continuously produced. N new particles are generated per time step at a cell face along an inflow boundary.

$$N = \frac{A\Delta t}{W_p} N_{\mathrm{i}} \tag{2}$$

where A is the face area, W_{p} the particle weight, and N_{i} the inflow number flux computed as

$$N_{\mathrm{i}} = \frac{nV_m\{\exp(-s^2\cos^2\beta) + \sqrt{\pi}s\cos\beta[1+\mathrm{erf}(s\cos\beta)]\}}{2\sqrt{\pi}} \tag{3}$$

where n is the inflow number density, V_{m} the average thermal speed, erf(·) the error function, s speed ratio, and β reciprocal of the most probable molecular speed in an equilibrium gas. The inlet particle distribution follows an equilibrium velocity distribution at the inflow condition.[15]

2.2.2. PWS software

There are some excellent software programs for plume numerical research, such as Icarus in USA,[21] SMILE in Russia,[22] MONACO in USA, and DS3V in Australia.[23] These software programs have been used for many actual space missions for plume effects studies.

The DSMC-based PWS (Plume WorkStation) software is the general simulation software developed by BUAA. The software is modularized, which includes initial condition module, boundary condition module, parameter module and mesh generating module. These modules can transfer all kinds of parameters into the format adopted in the software, and then process the data processing and control interface.

The uniform data process and control interface provide a man–machine conversation environment. Users can make further modification and set the operation process on the interface. The kernel of PWS is plume calculation methods described above.

2.3. Parallel calculation

The physical nature of the DSMC method leads to high computational expense. Using parallel calculation can greatly accelerate calculation speed and enlarge the usable memory resources. In order to demonstrate the capability of the parallel DSMC program, the typical axially-symmetric and 3D numerical simulations for 10 N thruster plume on DFH-3 satellite were carried out. The computational region was chosen as 300 mm × 200 mm and 300 mm × 200 mm × 280 mm respectively.

Fig. 1(a) shows the speed-up ratio of parallel calculation in the axially-symmetric case, and Fig. 1(b), the speed-up ratio of parallel calculation in the three-dimensional case. In the two figures, X-axis is the number of nodes p and Y-axis is the speed-up ratio S_{p}. Fig. 1 indicates that as the number of processors increases, nearly linear speed-up can be achieved. Fig. 2 shows the comparison of results between the parallel DSMC calculation and the serial calculation. It can be seen that the calculation results of parallel DSMC (PDSMC) calculation are consistent with the results of serial calculations.

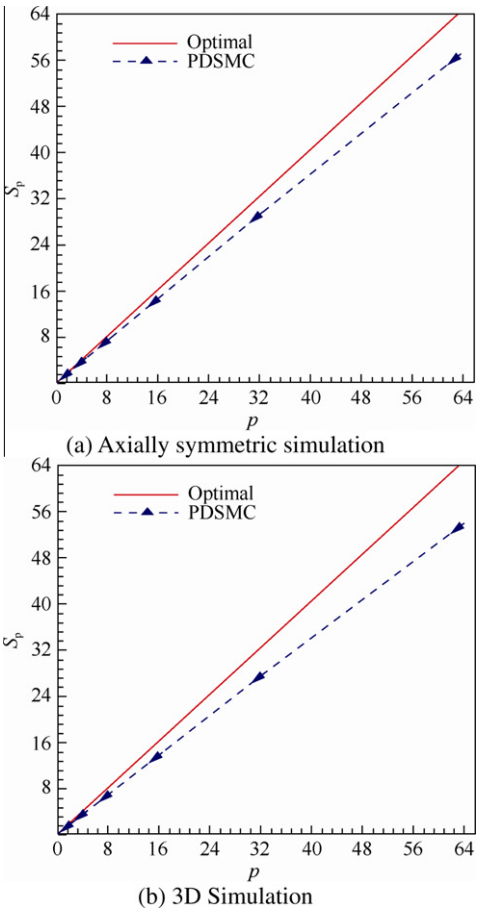

Fig. 1 Parallel computation speed-up ratio.

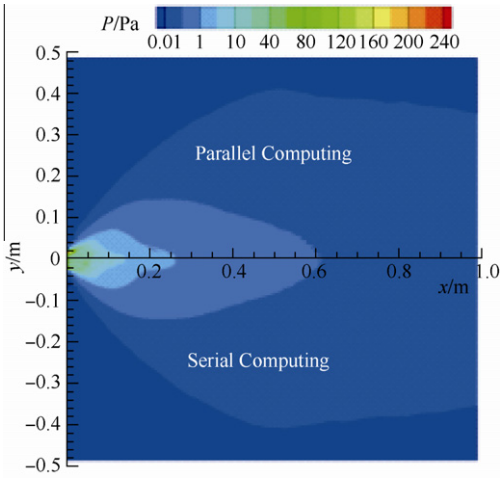

Fig. 2 Pressure comparison between serial and parallel calculations.

3. Experimental studies

In order to validate the DSMC software and obtain the actual plume parameters of attitude control thrusters, experimental studies of vacuum plume were carried out in China Aerodynamics Research and Development Center.

The experiment was conducted in the supersonic low density wind tunnel, which can simulate high-altitude environment from 60 to 90 km. This wind tunnel consists of gas supply system, pressure adjustment system, front chamber, nozzle, test section, pressure enlargement section, cooling section, vacuum system and measurement system. The plume test equipment includes the gas supply system, graphite resistance heater, test section and vacuum system. The high-temperature water-cooling pipelines are set up between graphite resistance heater and test section.

3.1. Plume field parameters

The cold and ignited nitrogen was chosen to be the experiment gas. The plume field parameters were measured by a pitot tube. The local Mach number and static pressure were obtained from the pitot pressure. The whole plume structure was displayed through glow discharge method. In order to study the effects of the nozzle type, cone-shaped nozzle and bell-shaped nozzle were adopted.

3.1.1. Model thruster nozzle

Two conical nozzles were selected as the investigation objects. Cold nitrogen was selected as the test gas. The small thrusters' geometry parameters are listed in Table 1. Five different cases were tested and plume parameters were measured. The experiment conditions are shown in the Table 2, where P_0 and T_0 are the total pressure and temperature respectively.

Table 1 Nozzle geometry of model thruster nozzle.

Item	Nozzle 1	Nozzle 2
Thrust F (N)	2	2
Inlet diameter D_i (mm)	10	10
Throat diameter D_t (mm)	1.2	1.2
Scarf	No	45°
Exit diameter D_e (mm)	8.5	8.5
Inlet half angle θ_i (°)	23.75	23.75
Exit half angle θ_e (°)	15	15

Table 2 Experimental conditions.

Case	Nozzle	P_0 (MPa)	T_0 (K)
1-1	1	1.0	300
1-2	1	0.5	300
1-3	2	1.0	300
1-4	2	0.5	300
1-5	2	0.11	300

Fig. 3 shows the plume structures in Case 1-1 and Case 1-3. It indicates that the plume field of cone-shaped nozzle was relatively simple and clear, and its shape looks like feathers. N_2 was ejected from the nozzle and expanded into low-pressure environment. The boundary of plume was characterized by expanding waves with paraboloid shape. No shock wave was generated in the flow field. Plume boundary expanded more widely when the nozzle nominal thrust increased.

Pitot pressure was measured by setting Pitot tube at different locations along nozzle axis. Fig. 4 shows measurement results of pitot pressure for different cases, in which the pressure of plume decreases along the nozzle axis. P_0 is the pressure at the nozzle exit. The pitot pressure is normalized by the value of P_0.

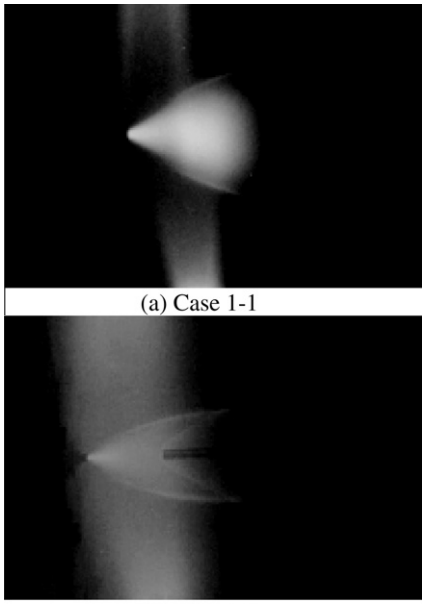

Fig. 3 Plume field structure of model thruster nozzle.

The Mach number of flow field can be obtained from total pressure P_0 and pitot pressure P_{t2}. The expression is

$$P_{t2} = P_0\left(\frac{2\gamma}{\gamma+1}Ma_1^2 - \frac{\gamma-1}{\gamma+1}\right)^{-\frac{1}{\gamma-1}} \cdot \left[\frac{(\gamma+1)Ma_1^2}{(\gamma-1)Ma_1^2+2}\right]^{\frac{\gamma}{\gamma-1}} \quad (4)$$

where γ is ratio of specific heat. The measurement pressure of pitot tube in hypersonic flow field can be calculated from

$$\frac{P_{t2}}{P_1} = K^*\left[\frac{2K^{*2}Ma_1^{2\gamma}}{2\gamma Ma_1^2+1-\gamma}\right]^{\frac{1}{\gamma-1}} \quad (5)$$

where $K^* = (\gamma + 1)/2$, and the subscripts 1 and 2 represent a shock ahead and behind parameter respectively. Local static pressure can be gained using Eq. (6).

Fig. 5 shows the results of static pressure along the nozzle axis for different cases. The figures indicate that the pressure drops along the axis while the Mach number increases monotonously along the axis.

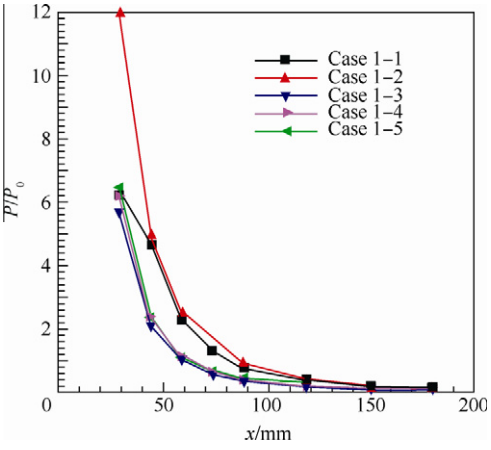

Fig. 4 Pitot pressure distribution along the axis of model thruster nozzle.

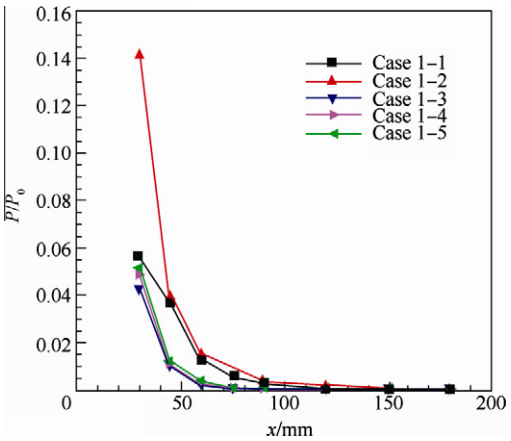

Fig. 5 Static Pitot pressure distribution along the axis of model thruster nozzle.

The experimental Case 1-1 was calculated using PWS numerical simulation software. The supersonic low density wind tunnel could simulate the environment of over 60 km altitude, where it is not absolute vacuum. So the environment pressure should be considered during the numerical simulation. Four different background pressures (i.e. 1, 4, 20 Pa, and vacuum conditions) were taken into account. Fig. 6 shows the plume density contour, while Fig. 7, the pressure comparison between computational and experimental results along the axis. The comparison between different back pressure conditions shows that environment pressure has little effect on the parameters along the axis. The results obtained from PWS generally agree well with the experimental data of the model thrusters, although the numerical simulation results are a little smaller than experimental ones (Fig. 7).

3.1.2. Attitude control thruster nozzle

In order to simulate plume of the real satellite attitude control thrusters, ignited flow experiments were carried out. The plume parameters of two 10 N thrusters were selected as the investigation objects. The thrusters' geometry parameters are listed in Table 3. These 10 N attitude control thrusters were used for DFH-3 and DFH-4 satellites. Experimental conditions are listed in Table 4.

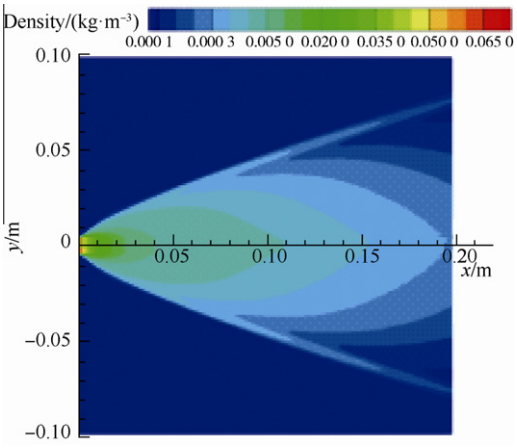

Fig. 6 Density contour of model thruster nozzle (Case 1-1).

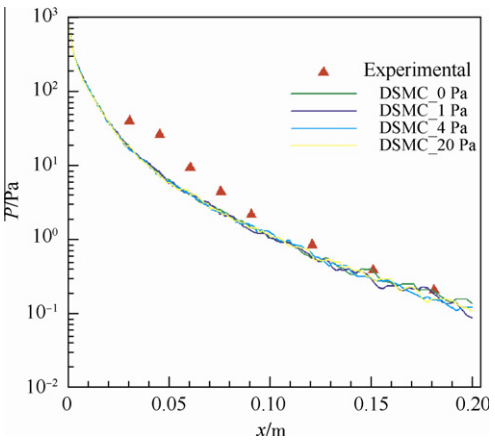

Fig. 7 Pressure contrast between DSMC and Experimental results on the axis (Case 1-1).

Table 3 Nozzle geometry.

Item	Nozzle 1	Nozzle 2
Expansion ratio	200	100
Exit diameter D_e (mm)	42.6	29.4

Table 4 Experimental cases.

Case	Nozzle	P_0 (MPa)	T_0 (K)
2-1	1	0.8	773
2-2	1	0.1	773
2-3	2	0.8	773
2-4	2	0.1	773

Fig. 8 shows the plume field structures of Case 2-1 and Case 2-3 respectively. For Fig. 8(a) and (b), the pressure measure rakes were placed at 250 and 245 mm away from the nozzle

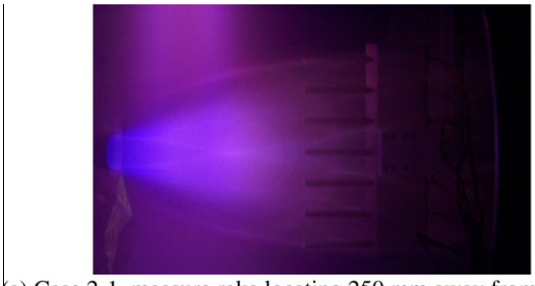

(a) Case 2-1, measure rake locating 250 mm away from nozzle exit plane

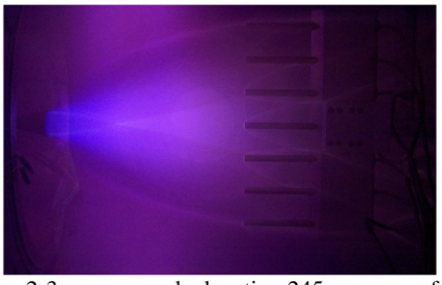

(b) Case 2-3, measure rake locating 245 mm away from nozzle exit plane

Fig. 8 Plume field structure of satellite attitude control thruster nozzle.

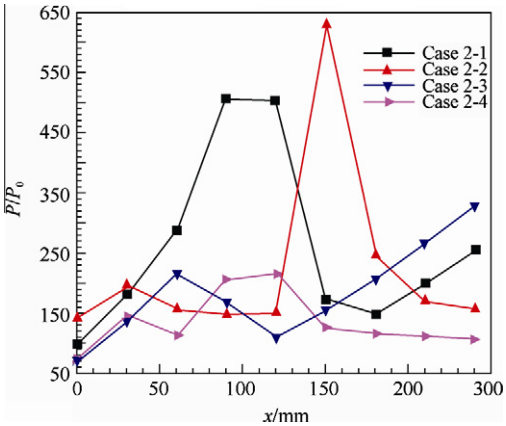

Fig. 9 Pitot pressure along the axis of satellite attitude control thruster nozzle.

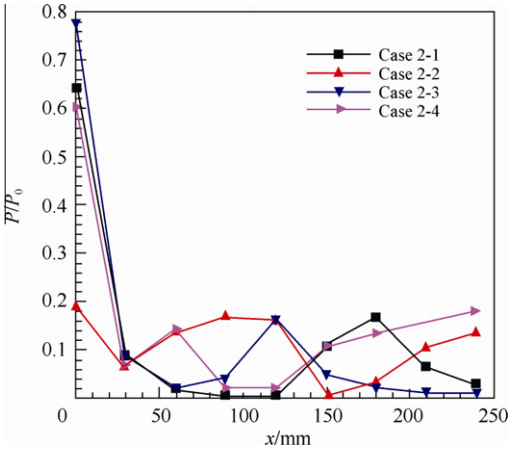

Fig. 10 Static pressure along the axis of satellite attitude control thruster nozzle.

exits. High temperature N_2 expanded into the high-vacuum environment after it is ejected from the nozzle. Expanding waves with paraboloid shape formed the boundary of the plume. The bell shaped profile of the nozzle caused a cone shock wave. This cone shock wave formed another cone shock wave after convergence. As the pressure of the nozzle frontal room rises, the junction point moved backwards and plume boundary enlarges. Backflow did not form, because the vacuum degree of the environment was not high enough to form backflow.

From the contrast between the plume structure of the cone-shaped nozzle (Fig. 7) and that of the bell-shaped nozzle (Fig. 8), it can be found that different nozzle profiles cause different flow structures.

In order to detect the more complex plume field of the bell-shaped nozzle, pressure probes, which were fixed on a flat was used to measure the flow pressure. There were 9 probes on the pressure measure rake and the distance between two probes was 40 mm. Since the expanding region was small near the nozzle, there were 1 or 3 probes locating in the flow field. Besides, the total time elapsed just 90 s during each test and the distance of the probe motion along the axis was limited within the flow field, it could not measure elaborately flow field structure, such as the exact location of shock wave and detailed Mach number distributing of ahead or behind shock wave. Because the probe at the plume axis was always in the flow field and the measure results were comparatively steady, the axis parameters were chosen as final experimental results.

The pressure and Mach number results could reflect the plume flow field structure comparatively factual. Figs. 9 and 10 show measurement results along the axis for each case. Measured results of pitot pressure are showed in Fig. 9. Through data processing, Fig. 10 illustrates the pressure along the plume axis of the experimental measurement respectively. The horizontal axis starts from the nozzle exit. It can be shown that the pressure values along the axis first fell and then rose up and then fell again. The Mach number first rose up and then fell. The trends are due to the fact that the gas expanded in the high-vacuum environment after the gas was ejected from the nozzle, which agrees with the conclusions in Ref.[24] At the same time, its velocity increased while pressure fell. Since the nozzle is a bell-shaped nozzle, once the gas crosses the cone-shaped shock wave, the gas is compressed, the velocity decreases and the pressure rises up. Then, the gas continues expanding and the velocity increases.

As discussions above, the environment pressure has fewer effects on the pressure value at the plume field axis and has a great effect on plume expanding extent. The lower environment pressure is, the more obviously plume expands.

Fig. 11 shows the flow pressure distribution result calculated by PWS, and Fig. 12, the contrast between the calculation results and the experiment results. It can be found that the DSMC results capture the shock wave position well, and the calculated pressure values agree with experiment results well. The validation work shows the feasibility and the reliability of PWS again.

3.2. Aerodynamic force experiments

Aerodynamic force experiments were carried out in the supersonic wind tunnel at CARDC.

The satellite attitude control thruster nozzle was chosen as the experimental object and a flat plate was laid near the nozzle to investigate the plume aerodynamic force. The distance

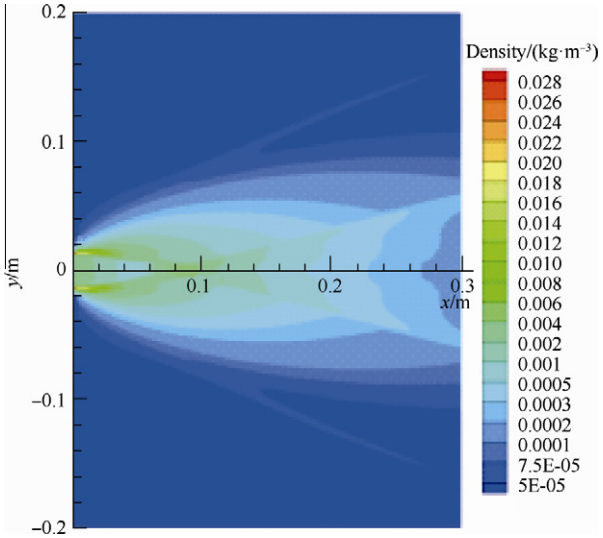

Fig. 11 Plume pressure (Case 2-3) of satellite attitude control thruster nozzle.

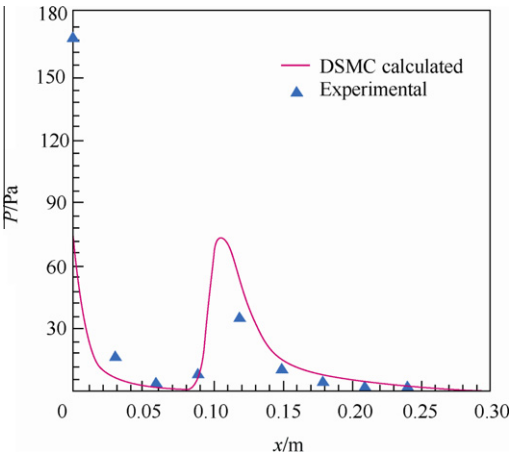

Fig. 12 Contrast between DSMC result and experiment of satellite attitude control thruster nozzle (Case 2-3).

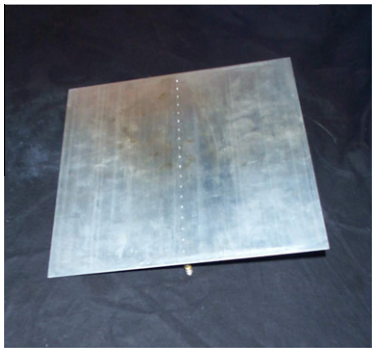

Fig. 13 Flat plate model for impingement force.

between the nozzle and the plate and their angles can be adjusted in order to simulate the installation location of thrusters on satellites. Measurement results give the pressure distribution on the plate.

The geometry parameters of satellite attitude control thruster nozzles are listed in Table 3. Fig. 13 is the flat plate model for the plume impingement force, which is 300×300 mm. The material of the plate is aluminum. There are 19 holes for pressure measurement with $\varnothing$ 2 mm. The distance between two holes is 15 mm. The distance from the first hole to the front of the flat plate model is 15 mm. Fig. 14 shows the picture of

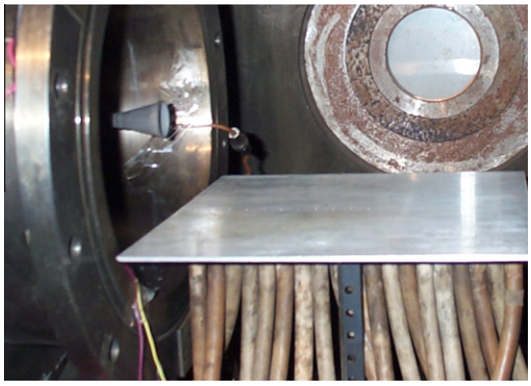

Fig. 14 Impingement force measurement.

Table 5 Experimental cases for plume impingement force of satellite attitude control thruster nozzle.

Case	Nozzle	P_0 (MPa)	T_0 (K)	z (mm)
3-1	1	0.8	773	40
3-2	1	0.1	773	40
3-3	1	0.8	773	80
3-4	1	0.1	773	80
3-5	2	0.8	773	40
3-6	2	0.1	773	40
3-7	2	0.8	773	80
3-8	2	0.1	773	80
3-9	1	0.8	773	0
3-10	1	0.8	773	5

plume impingement force measurement, which was measured with pressure sensors.

Eight cases in Table 5 for plume impingement force were measured for two different satellite attitude control thrusters. The complex structure was formed when the plume impinged the flat plate model, which is a 3D structure (see Fig. 15). Peaks of impingement force exited on the surface of flat plate. In Fig. 15, the shock wave in the plume is obvious to observe, which was generated due to the shape of the nozzle, and it is a characteristic for the 10 N satellite attitude control thruster nozzles.

The impingement force measurement results are shown in Fig. 16. The top one is the 2D distribution results and the right is the surface pressure measurement. It could be seen from the picture that there are peaks of force on the surface. The value at the centerline is higher than other locations. Because the nozzle is bell-shaped, the shock wave is formed and it would bring about some pressure peaks.

The flow structure indicated that complicated wave structure appeared after impingement and shock wave appeared on the interface between the edge of plume and the plate. The shock wave was protuberant in the center and pinched into camber on both sides. It contacted with shock wave in plume field and then entered pressure enlargement section.

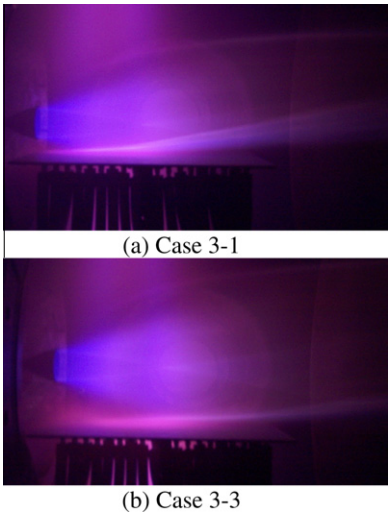

Fig. 15 Plume field structure of satellite attitude control thruster nozzle.

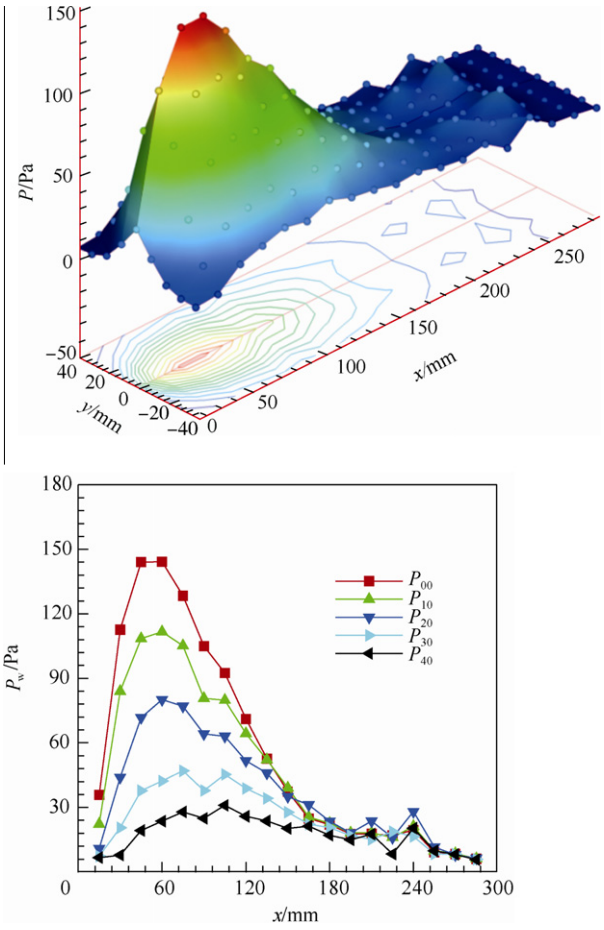

Fig. 16 Impingement pressure of satellite attitude control thruster nozzle.

After plume impinged the plate, it produced a longitudinal shock wave and transverse shock wave. Both shock waves bended upwards. Peak value of aerodynamic force existed in the plate surface.

3.3. Aerodynamic thermal experiments

Aerodynamic thermal effects of attitude control thruster nozzle were measured in high supersonic low density wind tunnel at CARDC. Aerodynamic thermal effects were simulated in hot flow case.

Fig. 17 shows the flat plate for plume heat load, whose dimension is the same as the model for force investigation but the material is 1Cr18Ni9Ti. There are 19 holes for temperature measurement with ∅ 0.5 mm and the locations are also the same as those of the force investigation model. Fig. 18 is the model for backflow heat flux measurements and the material is 1Cr18Ni9Ti. There are 5 holes for heat flux measurement with ∅ 0.3 mm. The distance between two holes is 7.5 mm. The distance from the first hole to the front is 7.5 mm.

Fig. 19 is the picture of plume heat load measurement, which was measured using thermocouples. Fig. 20 is the picture of plume backflow heat flux measurement, which was measured also using thermocouples.

The formula for heat flux is[23]

$$\dot{q}_W = \rho \cdot c \cdot b \cdot \frac{dT}{dt} \tag{6}$$

where $\dot{q}_W$ is the heat flux on the flat plate surface and its unit is W/m^2. ρ is the density of model, c the specific heat of model,

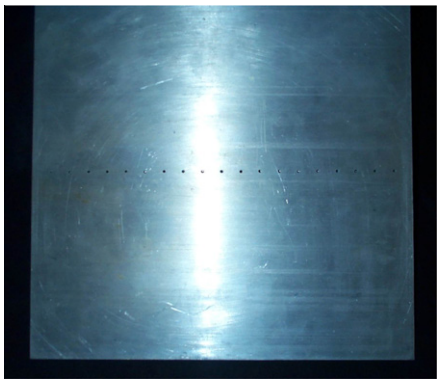

Fig. 17 Flat plate for heat load investigation.

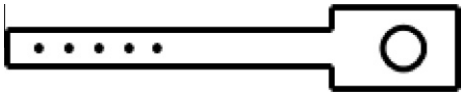

Fig. 18 Model for backflow heat flux investigation.

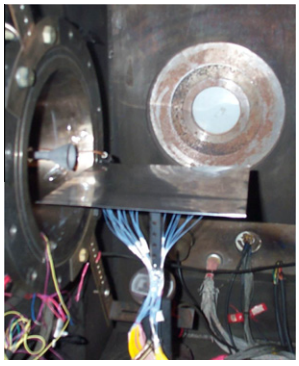

Fig. 19 Heat load measurement.

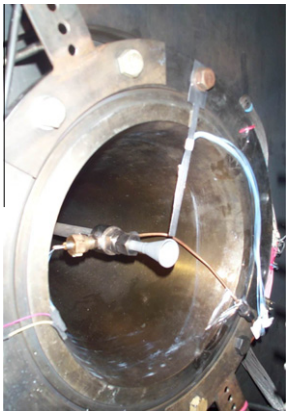

Fig. 20 Backflow heat flux measurement.

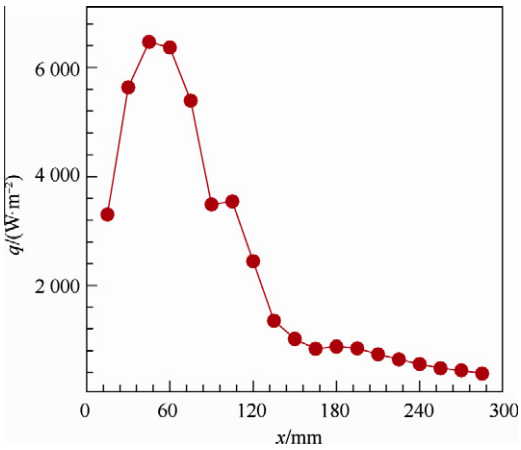

Fig. 21 Impingement heat load of satellite attitude control thruster nozzle for Case 3-9.

and b the thickness of model. For the experiment of heat flux, the material is 1Cr18Ni9Ti; therefore, the density is equal to 7.9×10^3 kg/m^3, the specific heat is equal to 500 J/(kg °C), and the thickness is 5×10^{-4} m. Thus, the formula can be deduced:

$$\dot{q}_{\mathrm{W}} = 1975 \cdot \frac{\mathrm{d}T}{\mathrm{d}t} \quad \mathrm{W/m^2} \tag{7}$$

The aerodynamic thermal load result is shown in Fig. 21. Fig. 22 shows experimental results of heat flux along the nozzle axis after the plume impact plate model, which are just on the centerline. From Fig. 21, it could be seen that the trend of heat flux distribution is consistent with that of plate surface pressure. After the plume impacts the plate, the heat flux reaches the peak value. After the heat flux reaches the peak, the curve declines along the centerline of plate constantly. The maximal heat flux is about 6 300 W/m^2.

Fig. 22 shows the backflow heat load result. As for nozzle 1, the total pressure is 8.0×10^5 Pa and the total temperature is 773 K. The distance between the edge of baffle and the exit of nozzle is 5 mm. The experimental results of heat flow distribution for model surface are shown in the figure. The maximal surface heat flux of model is about 580 W/m^2. The surface heat flux of model declines along the axis of nozzle. It appears that the shorter the distance from the nozzle exit, the bigger the heat flux is. In view of the picture of plume structure, the conclusion that the backflow was not formed could be brought forward. The result of this experiment could not explain why there was a backflow, for the radiation of hot nozzle wall could possibly yield the same results.

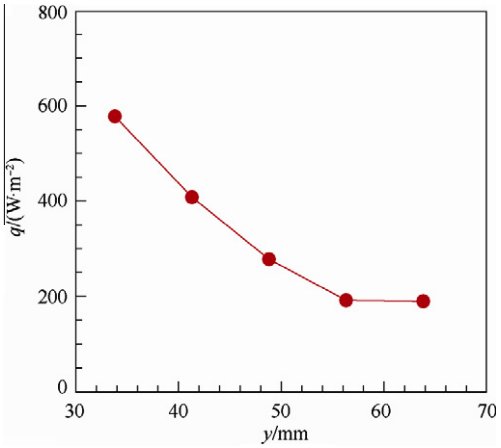

Fig. 22 Backflow heat load of satellite attitude control thruster nozzle for Case 3-10.

4. Conclusions

(1) In this paper, numerical simulation and experiment researches on vacuum plume and its effects are introduced. In numerical simulation, a strategy that combines the N–S equations solutions and the DSMC method are adopted to solve the plume field. N–S equations are applied to solving the nozzle internal flow. The DSMC method is applied to calculating plume field. In order to overcome the time-consuming and large memory difficulties, the parallel DSMC calculation is also developed. A general DSMC-based simulation software system called PWS (Plume WorkStation) software is introduced by BUAA. To verify the parallel calculation module, the plume field of 10 N thruster is simulated by the axially symmetric and 3-D DSMC method.

(2) In order to verify the PWS and investigate the plume and its effect, experimental studies are carried out in a supersonic low density wind tunnel which could simulate the 60–80 km altitude environment. During the experiments, the parameters of plume field and aerodynamics forces and heat load are measured. Several different experimental conditions and different nozzles are considered. Both the plume impingement forces and heat load with two 10 N attitude control thrusters are measured through experiments which use the heated nitrogen to simulate the real working process of the attitude control thrusters. The heat flux of baffle in the backflow is tested through a specially designed project. Results of the measurement could provide the reference for backflow analysis.

In conclusion, this paper introduces all the researches on vacuum and its effects conducted by Beihang University, including the numerical and experimental investigations for the practical satellite attitude control thruster working process and plume's effects. Future work concerning plume effects will be conducted based on more advanced experimental systems.

References

1. Simons GA. Effect of nozzle boundary layers on rocket exhaust plumes. *AIAA J* 1972;**10**(11):1534–5.
2. Albini FA. Approximate computation of underexpanded jet structure. *AIAA J* 1966(8).
3. Bird GA. *Molecular gas dynamics and the direct simulation of fas flows*. Oxford: Clarendon Press; 1994.
4. Boyd ID, Penko PF, Carney LM. Efficient Monte Carlo simulation of rarefied flow in a small nozzle. 1990. Report No.: AIAA 90-1693.
5. Dettleff G, Plahn K. Initial experimental results from the new DLR-high vacuum plume test facility STG. 1997. Report No.: AIAA 97-3297.

6. Plahn K, Dettleff G. Modeling of N_2-thruster plumes based on experiments in STG. In: *Rarefied Gas Dynamics 22nd International Symposium*; 2000 July 9–14; Sydney. 2000. p. 848–855.
7. Boyd ID, Penko PF, Meissner DL, DeWitt KJ. Experimental and numerical investigations of low-density nozzle and plume flows of nitrogen. *AIAA J* 1992;**30**(10):2453–61.
8. Koontz S. Shuttle plume impingement experiment Internet. 2006 May [cited 2011 October 1]. Available from: <http://else-s1.msfc.nasa.gov/seeindex.html>.
9. Ashkenas H, Sherman FS. The structure and utilization of supersonic free jets in low density wind tunnels. *Rarefied gas dynamics, fourth symposium*, vol. II. New York: Academic Press; 1966. p. 84–105.
10. Penko PF, Boyd ID, Meissner DL, DeWitt KJ. Measurement and analysis of a small nozzle plume in vacuum. 1992. Report No.: AIAA 92-3108.
11. Ivanov MS, Markelov GN. Numerical study of thruster nozzle plume. 2000 Jan. Report No.: AIAA-2000-0468.
12. Cai GB, Wang HY, Zhuang FG. Numerical simulation on vacuum plume and numerical analyzing study on vacuum plume contamination. *J Astronaut* 1998;**19**(3):1–9 Chinese.
13. Giordano D, Ivanov MS, Kashkovsky A, Markelov G, Tumino G, Koppenwallner G. Application of DSMC to the study of satellite thruster plumes. 1997. Report No.: AIAA 97-2538.
14. Baldwin B, Lomax H. Thin-layer approximation and algebraic model for separated turbulent flows. 1978. Report No.: AIAA 78-257.
15. Koura K. Null-collision technique in the DSMC method. *Phys Fluids* 1986;**29**(11):3509–11.
16. Koura K. Transient couette flow of rarefied binary gas mixtures. *Phys Fluids* 1970;**13**(6):1457–66.
17. Ivanov MS, Rogazinskii SV. Comparative analysis of algorithms of DSMC in rarefied gas dynamics. *Comput Math Math Phys* 1988;**28**(4):63–71.
18. Bird GA. Perception of numerical methods in rarefied gas dynamics. In: 16th Symposium on Rarefied Gas, Dynamics; 1988. p. 211–226.
19. Fan J, Shen C. A new arithmetic of the direct simulation Monte Carlo – randomly sampled frequency method (RSF)*Theory, method and application of CFD*. Beijing: Science Press; 1992. p. 127–8.
20. Bartel T, Plimton S, Gallis MA. Icarus: A 2-D DSMC code for multi-processor computers. Users' Manual V10.0. Sandia Report, SAND 2001-2901.
21. Ivanov MS, Markelov GN, Gimelshein SF. Statistical simulation of reactive rarefied flows: numerical approach and applications. 1998. Report No.: AIAA 98-2669.
22. Bird GA. Direct simulation Monte Carlo method visual programs at GAB consulting Internet. 2006 May [cited 2011 October 1]. Available from: <http://ourworld.compuserve.com/homepages/gabird>.
23. Khasawneh K, Liu HL, Cai CP. Surface properties for rarefied circular jet impingement on a flat plate. *Phys Fluids* 2011;**23**: 1–6.

He Bijiao is a lecturer at School of Astronautics, Beihang University. He received the Ph.D. degree from the same University in 2009. His research interest is the vaccuum plume and control technology.

Cai Guobiao is a professor and Ph.D. supervisor at School of Astronautics, Beihang University. He received the Ph.D. degree from the same University in 1996. His research interests include the vacuum plume effects and control technology, the rocket engine optimization and simulation techniques, the rocket engine re-use technology and hybrid rocket engine technology and application.